

# Non-equilibrium phase transition in relativistic nuclear collisions: Importance of the equation of state

Jan Steinheimer,<sup>1,2,\*</sup> Jørgen Randrup,<sup>1,†</sup> and Volker Koch<sup>1,‡</sup>

<sup>1</sup> Nuclear Science Division, Lawrence Berkeley National Laboratory, Berkeley, California 94720, USA

<sup>2</sup> Frankfurt Institute for Advanced Studies, Johann Wolfgang Goethe Universität,  
Ruth-Moufang-Straße 1, 60438 Frankfurt am Main, Germany

(Dated: July 22, 2018)

Within the context of relativistic nuclear collisions aimed at exploring hot and baryon-dense matter, we investigate how the general features of the expansion dynamics, as well as a number of specific observables, depend on the equation of state used in dynamical simulations of the non-equilibrium confinement phase transition.

## I. INTRODUCTION

One of the central themes of current research in strong-interaction physics is the exploration and characterization of strongly interacting matter at high temperatures and/or densities. In the laboratory, strongly interacting matter at high temperature and density is created in collisions of heavy nuclei at relativistic energies and experiments to study these reactions are carried out at various accelerator facilities, particularly the Relativistic Heavy Ion Collider (RHIC) at BNL and the Large Hadron Collider (LHC) at CERN. In the universe, strongly interacting matter at high density but very low temperature may exist in the core of neutron stars, and its properties control the maximum mass and radius of those stars.

Experiments at RHIC and LHC have demonstrated that collisions at nucleon-nucleon center-of-mass energies of  $\sqrt{s_{NN}} \geq 60$  GeV create matter at very high temperature  $T$  and nearly vanishing net-baryon density,  $\rho$ , i.e.  $\rho/T^3 \ll 1$ . Recent continuum-extrapolated lattice QCD calculations with physical quark masses show that such matter exhibits a crossover transformation from an interacting hadronic gas to a quark-gluon fluid at a pseudo-critical temperature of  $T_x \simeq 155$  MeV [1–3].

Nuclear collisions at lower energies produce systems at finite net-baryon densities with the corresponding baryon-number chemical potential  $\mu$  being of the order of the temperature or higher. This region is difficult to explore with lattice QCD techniques due to the fermion sign problem but for sufficiently small values of  $\mu/T$  the pressure may be expanded in powers of  $\mu/T$ , providing a hint about the finite- $\mu$  behavior [4–8]. Alternative methods use an imaginary chemical potential [9] or apply re-weighting techniques [10, 11]. However, all these approaches are restricted to small values of  $\mu$  and have limited predictive power at the large chemical potentials. The theoretical exploration to higher net baryon densities must therefore rely on models.

Among the many effective models for QCD thermodynamics, those that couple constituent quarks to mesonic fields and the Polyakov loop have become popular because they include chiral-symmetry breaking and a "thermal" confinement of quarks. Such approaches are the Polyakov Nambu–Jona-Lasino (PNJL) [12, 13] and the Polyakov Quark-Meson (PQM) [14] models. Recently also results based on functional renormalization group (FRG) approaches have been investigated [15–18]. These models can be brought into agreement with lattice results at vanishing net baryon density but their results for the finite-density domain depend significantly on the parametrizations used. A particular weakness in most of these models is the absence of explicit hadronic degrees of freedom in the confined phase. There exist only few examples where the equations of state (EoS) includes an approximately realistic description of the hadronic phase. These equations of states are constructed either by matching a purely hadronic model to an MIT-bag EoS or by combining a PNJL/PQM-type model with a chiral hadronic model [19, 20]. Obviously, these models need to be constrained both by lattice QCD results at zero and small chemical potential and by known properties of nuclear matter at small temperatures and densities up to about twice nuclear matter density [21], as well as by astrophysical observations on neutron star properties [22].

As already discussed in [23] there is a qualitative difference between the various effective models that do not include explicit hadronic degrees of freedom and those which include the hadronic degrees of freedom. Many of the aforementioned Polyakov loop models, as well as various incarnations of the linear sigma model and Nambu–Jona-Lasino model [24], belong to the former group. These models typically predict coexistence between the (deconfined and/or chirally symmetric) dense phase and the vacuum at vanishing temperature. Consequently the coexistence pressure at  $T = 0$  vanishes and, as a result, it remains small even at moderate temperatures. This unrealistic behavior is akin to the well known liquid gas phase transition and subsequently we will refer to models in this group as LG models. In reality, however, at vanishing temperature the (deconfined and/or chirally symmetric) dense phase coexists with compressed nuclear matter. Therefore the coexistence pressure is finite and

---

\*Electronic address: steinheimer@fias.uni-frankfurt.de

†Electronic address: JRandrup@LBL.gov

‡Electronic address: VKoch@LBL.gov

large. Indeed, as will be discussed below, it will likely be larger than the (pseudo) critical pressure at vanishing net-baryon density. This qualitative difference between LG models and more plausible models will lead to qualitative differences for the expansion dynamics of the system, as we shall show.

Experimentally, different regions of the phase diagram of strongly interacting matter can be explored with nuclear collisions by varying the energy, thereby influencing the phase trajectory along which the bulk of the created system evolves [25]. However, the successful discovery of a phase transition requires the measurement of suitable observables that are sensitive to such a structure in the phase diagram. Since the identification of signal observables is a challenging task, due to the complexity of the collision, one must invoke dynamical simulations. It is, therefore, essential to develop transport models that are capable of describing the evolution of the system in the presence of a phase transition, in particular propagate it correctly under the influence of the associated mechanical instabilities [26–34]. Such a dynamical model was recently presented [35, 36] and the present work uses it to explore the sensitivity of various observables to the presence of a first-order coexistence region in the phase diagram.

The purpose of the present paper is twofold: First we wish to explore the qualitative differences between LG-type equations of state and the more plausible ones that have phase coexistence between compressed nuclear matter (rather than vacuum) and a denser (deconfined and/or chirally symmetric) phase. In particular we are interested in generic differences in the fluid dynamic time evolution. To this end we will study two illustrative equations of state that serve as representatives for the two types of models, LG and “realistic”, as discussed above. The second purpose of the paper is to elucidate the sensitivity of various observables to the existence of a first-order phase coexistence region and its associated instabilities.

Because we will be working in the framework of fluid dynamics, the only relevant information is the equation of state. Therefore, our results will not discriminate between a phase transition driven by chiral restoration or one driven by deconfinement. Therefore we will subsequently refer to the (deconfined and/or chiral symmetric) dense phase simply as the quark phase (QP). Finally, we will restrict our studies to situations with only one first-order coexistence region in the phase diagram. The potentially interesting case of separate chiral and deconfinement transition will be left for future work.

The presentation is organized as follows: In the next section, we compare an EoS with a hadron-quark-type phase transition with the EoS of a PQM model and discuss their qualitative differences, with a view towards identifying potential phase-transition observables. These two equations of state are then used to carry out various calculations with our dynamical model which consists of finite-density ideal fluid dynamics augmented by a gra-

dient term in the local pressure [35]. Based on these results, we discuss the suitability of the two models for semi-realistic tests of the sensitivity of various observables for the QCD phase structure. Specifically, we discuss the effects of the non-equilibrium phase transition on composite-particle production as well as two-particle angular correlations.

Throughout this paper, for notational simplicity, we denote net baryon density by  $\rho$  and the associated baryon-number chemical potential by  $\mu$ .

## II. THE HQ EQUATION OF STATE

To investigate the effects of the instabilities associated with a first-order phase transition between a hadronic gas and a quark-gluon plasma, we need to employ a suitable two-phase EoS (which we shall refer to as the HQ equation of state). Although significant progress has been made in understanding the thermodynamical properties of each of the phases separately, our current understanding of the phase coexistence region is not yet on firm ground. We therefore follow Ref. [38] and employ a conceptually simple approximate EoS obtained by interpolating between an ideal hadron gas, augmented by a  $\rho$ -dependent interaction energy, and an idealized quark-gluon plasma. As already noted in the Introduction, we view this EoS as a representative of those equations of state that exhibit phase coexistence between compressed nuclear matter and the dense quark phase.

Furthermore, as a reference, we subsequently define a partner EoS obtained by eliminating the instabilities by means of Maxwell constructions.

The confined phase is approximated as an ideal gas of pions, nucleons, and antinucleons, plus an interaction term, so the total hadronic pressure is of the form

$$p^H = p_\pi + p_N + p_{\bar{N}} + p_w . \quad (1)$$

The contributions from the various hadron species are

$$p_\pi(T) = -g_\pi T \int \frac{d^3k}{(2\pi)^3} \ln[1 - e^{-\epsilon_\pi(k)/T}] , \quad (2)$$

$$p_N(T, \mu_0) = g_N T \int \frac{d^3k}{(2\pi)^3} \ln[1 + e^{-(\epsilon_N(k) - \mu_0)/T}] , \quad (3)$$

$$p_{\bar{N}}(T, \mu_0) = g_N T \int \frac{d^3k}{(2\pi)^3} \ln[1 + e^{-(\epsilon_N(k) + \mu_0)/T}] , \quad (4)$$

where  $g_\pi = 3$ ,  $g_N = 2 \times 2 = 4$ , and  $\epsilon(k)^2 = m^2 + k^2$  with  $m_\pi = 140$  MeV and  $m_N = 940$  MeV. The net baryon density  $\rho^H = \rho_N - \rho_{\bar{N}} = \partial(p_N + p_{\bar{N}})/\partial\mu_0$  then follows,

$$\rho^H(T, \mu_0) = g_N \int_{m_N}^{\infty} \frac{p d\epsilon}{2\pi^2} \frac{\sinh \mu_0/T}{\cosh \mu_0/T + \cosh \epsilon/T} . \quad (5)$$

Finally, the interaction contribution is given by  $p_w(\rho) = \rho \partial_\rho w(\rho) - w(\rho)$ , where  $w(\rho) = [-A\rho/\rho_s + B(\rho/\rho_s)^2]\rho$  is the interaction energy density. The strength coefficients

$A$  and  $B$  have been adjusted so that nuclear matter saturates at  $\rho_s = 0.153 \text{ fm}^{-3}$  and the associated compression modulus is  $K = K_N + K_w = 300 \text{ MeV}$ ; the binding energy of nuclear matter is then also roughly reproduced [38]. The Fermi level  $\mu_0$  and the chemical potential  $\mu$  are related by  $\mu = \mu_0 + \partial_\rho w(\rho)/\partial \rho$  and the entropy density is then  $\sigma^H(T, \mu) = \partial p^H(T, \mu)/\partial T$ .

The deconfined phase was taken as an ideal gas of massless gluons and massless  $ud$  quarks with a bag constant  $B = 300 \text{ MeV/fm}^3$  [38],

$$p^Q = p_g + p_q + p_{\bar{q}} - B, \quad (6)$$

where  $p_g = g_g(\pi^2/90)T^4$  with  $g_g = 2 \times 8 = 16$  is the gluon pressure while the quarks and antiquarks contribute

$$p_q + p_{\bar{q}} = g_q \left[ \frac{7\pi^2}{360} T^4 + \frac{1}{12} \left(\frac{1}{3}\mu\right)^2 T^2 + \frac{1}{24\pi^2} \left(\frac{1}{3}\mu\right)^4 \right], \quad (7)$$

with  $g_q = 2 \times 3 \times 2 = 12$ . The net baryon density in the plasma is then

$$\rho^Q = \frac{\partial}{\partial \mu} p^Q(T, \mu) = \frac{2}{3} \left(\frac{1}{3}\mu\right) T^2 + \frac{2}{3\pi^2} \left(\frac{1}{3}\mu\right)^3, \quad (8)$$

while the entropy density is

$$\sigma^Q = \frac{\partial}{\partial T} p^Q(T, \mu) = \frac{74}{45} \pi^2 T^3 + 2 \left(\frac{1}{3}\mu\right)^2 T. \quad (9)$$

At zero temperature and zero chemical potential, the pressure of the nucleon gas vanishes while that of the quark gas is equal to  $-B$ . The confined phase is then the thermodynamically favored one. However, as the chemical potential is raised, the plasma pressure increases faster than the hadronic pressure, so the curves  $p^H(T = 0, \mu)$  and  $p^Q(T = 0, \mu)$  cross at a certain value of  $\mu$ , above which the deconfined phase is favored. This phase crossing procedure can be repeated for any temperature. As  $T$  is increased, the crossing value of  $\mu$  decreases steadily, becoming zero at  $T_{\text{max}}$ , above which  $p^Q$  is larger than  $p^H$  for any value of  $\mu$ .

For the construction of the two-phase equation of state, it is convenient to work in the canonical representation. Then the condition of phase coexistence, *i.e.* same temperature, chemical potential, and pressure at two different densities  $\rho_1$  and  $\rho_2$ , amounts to the condition that  $f_T(\rho)$ , the free energy density at a specified temperature as a function of density, exhibit a local concavity. The two coexistence densities are then those at the touching points of the associated common tangent. This is readily seen since  $\mu_T(\rho) = \partial_\rho f_T(\rho)$  implies that the two chemical potentials are then equal,  $\mu_T(\rho_1) = \mu_T(\rho_2)$ , and since the tangent at  $\rho_i$  is given by  $t_i(\rho) = f(\rho_i) + (\rho - \rho_i)f'(\rho_i)$  the fact that  $t_1(\rho) = t_2(\rho)$  immediately implies that also the pressures are equal,  $p_T(\rho_1) = p_T(\rho_2)$ .

At zero temperature, the hadronic free energy density,  $f_{T=0}^H(\rho)$ , starts at zero but grows more rapidly than the  $f_{T=0}^Q(\rho)$ , which starts at  $B$ . Therefore the two curves cross and, furthermore, because they both have positive

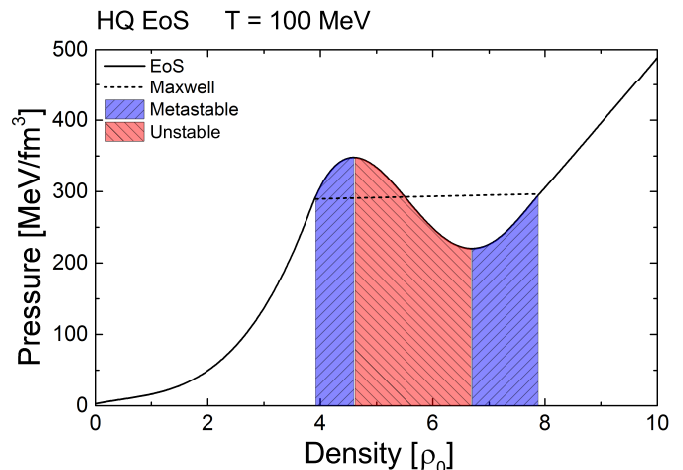


FIG. 1: (Color online) Illustration of the equation of state of the HQ model: The pressure  $p$  as a function of the net baryon density  $\rho$  at the fixed temperature  $T = 100 \text{ MeV}$  (solid curve) and the corresponding Maxwell construction (dashed line). The middle (red) shaded area shows the mechanically unstable density region while the adjacent (blue) shaded areas show the meta-stable regions (in which matter is mechanically stable but thermodynamically unstable).

curvature, a common tangent exists between two densities  $\rho_1$  and  $\rho_2$ . This feature signals the occurrence of phase coexistence. In order to describe the associated transition region, we follow Ref. [38] and employ a spline procedure. Thus, for each temperature below a critical value  $T_{\text{crit}} < T_{\text{max}}$ , we employ a set of matching densities,  $\rho_T^H < \rho_1$  and  $\rho_T^Q > \rho_2$ , which define three distinct density regions. The hadron EoS is used in the low-density region,  $f_T(\rho \leq \rho_T^H) = f_T^H(\rho)$ , the plasma EoS is used in the high-density region,  $f_T(\rho \geq \rho_T^Q) = f_T^Q(\rho)$ , and in the intermediate density region the free energy density is represented by a spline polynomial  $\tilde{f}_T(\rho)$  that matches the values, slopes, and curvatures of  $f_T(\rho)$  at  $\rho_T^H$  and  $\rho_T^Q$ .

By suitable adjustment of the matching densities, it is possible to obtain a resulting free energy density curve  $f_T(\rho)$  that displays an ever weakening phase transition as  $T$  is raised, up to a critical value,  $T_{\text{crit}} \approx 143 \text{ MeV}$ , above which the phase transformation occurs as a smooth crossover. The resulting pressure curve,  $p_T(\rho) = \rho \partial_\rho f_T(\rho) - f_T(\rho)$ , is shown in Fig. 1 for  $T = 100 \text{ MeV}$ .

In Ref. [38] the focus was on subcritical temperatures,  $T < T_{\text{crit}}$ , so for each  $T$  the spline points were adjusted so the resulting  $f_T(\rho)$  would exhibit a concave anomaly, ensuring that there would be two densities,  $\rho_1(T)$  and  $\rho_2(T)$ , for which the tangent of  $f_T(\rho)$  would be common, signaling phase coexistence. Ref. [35] extended the EoS to  $T > T_{\text{crit}}$  by using convex splines, as is characteristic of single-phase systems. Having constructed  $f_T(\rho)$  for a sufficient range of  $T$  and  $\rho$ , we may obtain the energy density,  $\varepsilon_T(\rho) = f_T(\rho) - T \partial_T f_T(\rho)$ , by suitable interpolation and then tabulate the EoS,  $p_0(\varepsilon, \rho)$ , on a convenient

Cartesian lattice in the mechanical densities  $\varepsilon$  and  $\rho$ .

### III. THE PQM MODEL

As an alternative, we shall also consider a Polyakov Quark Meson model as a representative of a class of models based on the coupling of constituent quarks to mesonic fields and the Polyakov loop. Other approaches of this type include the PNJL and FRG models in different realizations [12–14, 39–43]. These models have become quite popular because they include the correct degrees of freedom at high temperatures (namely weakly interacting quarks and gluons) and they have an effective thermodynamic description of the confinement transition and the chiral symmetry breaking that is in reasonable agreement with lattice results at  $\mu = 0$ . Within chiral fluid dynamics, this model has been recently applied in relativistic nuclear collisions for the purpose of investigating the effects of a first-order deconfinement transition and the critical endpoint [44, 45]. However, these models yield a rather poor description of the confined phase, as they allow for only (uncorrelated) three-quark states. Therefore, they typically severely underestimate the pressure in the hadronic phase, as we shall discuss subsequently. In addition, at zero temperature this type of model as well as sigma and NJL models [24] typically predict phase coexistence between the vacuum and the dense quark phase, similar to the well known liquid gas transition. We thus view the PQM model as a generic representative of LG-type models.

The effective thermodynamic potential of the PQM model can be written as

$$\Omega = -\frac{T}{V} \ln Z = \mathcal{U} + U_\sigma + \Omega_{q\bar{q}}. \quad (10)$$

The meson potential is given by

$$U_\sigma = \frac{1}{4}\lambda(\sigma^2 - \nu^2)^2 - c\sigma - U_0 + g_\omega\lambda_\omega^2\omega^2, \quad (11)$$

where the last term represents a repulsive interaction transmitted by the  $\omega$  vector field. The Polyakov-loop potential used in the present work is the logarithmic form introduced in Ref. [40],

$$\mathcal{U} = -\frac{1}{2}a(T)\Phi\Phi^* + b(T)\ln[1 - 6\Phi\Phi^* + 4(\Phi^3 + \Phi^{*3}) - 3(\Phi\Phi^*)^2], \quad (12)$$

with  $a(T) = a_0T^4 + a_1T_0T^3 + a_2T_0^2T^2$ ,  $b(T) = b_3T_0^3T$ . The parameters  $a_0 = 3.51$ ,  $a_1 = -2.47$ ,  $a_2 = 15.2$ , and  $b_3 = -1.75$  are fixed as in Ref. [40], and  $T_0 = 210$  MeV.

A coupling of the quarks to the Polyakov loop is introduced in the thermal energy of the quarks,

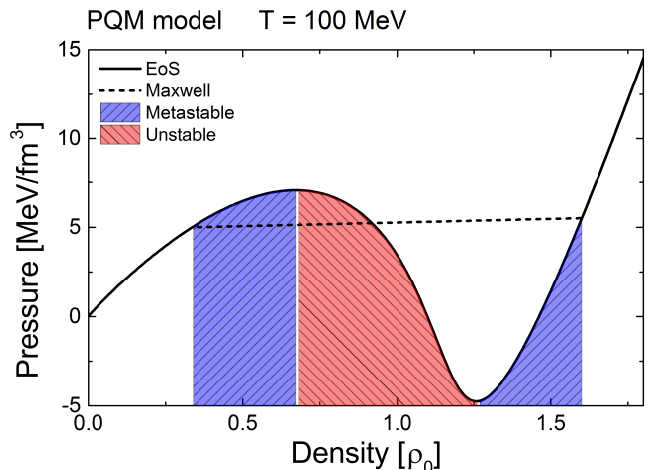


FIG. 2: (Color online) Illustration of the equation of state of the PQM model: The pressure  $p$  as a function of the net baryon density  $\rho$  at the fixed temperature  $T = 100$  MeV (solid curve) and the corresponding Maxwell construction (dashed line). The middle (red) shaded area shows the mechanically unstable density region while the adjacent (blue) shaded areas show the meta-stable regions (in which matter is mechanically stable but thermodynamically unstable).

$$\begin{aligned} \Omega_{q\bar{q}} = 2N_f \int \frac{d^3k}{(2\pi)^3} \left\{ T \ln \left[ 1 + 3\Phi e^{-(\epsilon(k) - \mu_q^*)/T} \right. \right. \\ \left. \left. + 3\Phi^* e^{-2(\epsilon(k) - \mu_q^*)/T} + e^{-3(\epsilon(k) - \mu_q^*)/T} \right] \right. \\ \left. + T \ln \left[ 1 + 3\Phi^* e^{-(\epsilon(k) + \mu_q^*)/T} \right. \right. \\ \left. \left. + 3\Phi e^{-2(\epsilon(k) + \mu_q^*)/T} + e^{-3(\epsilon(k) + \mu_q^*)/T} \right] \right\}, \quad (13) \end{aligned}$$

where only the light-quark flavors ( $u$  and  $d$ ) are included. The thermal heat bath of the quarks contains contributions from one-, two-, and three-quark states, of which only the latter do not couple to the Polyakov loop. The quark energy,  $\epsilon(k) = \sqrt{k^2 + m_i^{*2}}$ , includes the effective mass,  $m_i^* = m_0 + g_\sigma\sigma$  with  $m_0 = 6$  MeV, and the repulsive vector coupling leads to an effective chemical potential,  $\mu_q^* = \mu_q - g_\omega\omega$  that depends on the strength of the quark vector coupling  $g_\omega$ . The PQM model parameters used in this work are  $\lambda = 19.7$ ,  $\nu = 87.6$  MeV,  $c = 1.77 \cdot 10^6$  MeV<sup>3</sup>,  $\lambda_\omega = 500$  MeV,  $U_0 = 165 \cdot 10^6$  MeV<sup>4</sup>,  $g_\sigma = 3.2$ , and  $g_\omega = 0$  or  $g_\omega = 2$ .

For vanishing vector interaction strength,  $g_\omega = 0$ , the PQM model exhibits the desired phase structure, namely a smooth crossover at zero chemical potential as well as a first-order phase transition at zero temperature. The critical endpoint is located at  $\mu_{\text{crit}} \approx 480$  MeV and  $T_{\text{crit}} \approx 165$  MeV [14].

Using the PQM model, we can calculate a two-phase EoS, with an unstable region, by finding the local maxima (unstable states) and minima (meta-stable states) of the grand canonical potential. The resulting EoS is

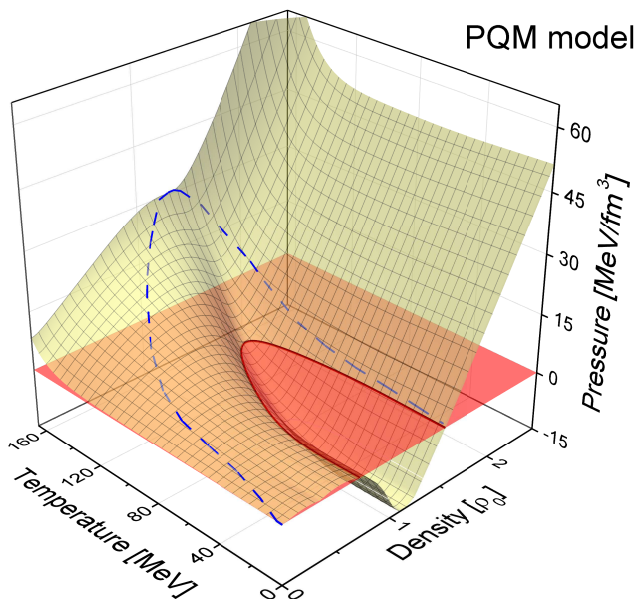


FIG. 3: (Color online) The PQM equation of state  $p(T, \rho)$ : The pressure as a function of both temperature and net baryon density. The phase-coexistence boundary is delineated (dashed path) and the plane of zero pressure is shown (red), making it easier to see where the pressure is negative.

illustrated in Fig. 2. It should be noted that the phase transition in the PQM model occurs at density and pressure values that are significantly lower than those of the HQ construction discussed above.

A more global impression of the PQM EoS (for  $g_\omega = 0$ ) can be obtained from Fig. 3 which shows  $p(T, \rho)$ , the dependence of the pressure on both temperature and baryon density. The pressure is negative in a large part of the phase coexistence region. It is also evident that at  $T = 0$  there is coexistence between the deconfined quark phase and the vacuum, a feature that will admit stable quark droplets in the vacuum. However, we know that the true ground state of matter, coexisting with the vacuum, is nuclear matter at saturation density and not quark matter. It will become apparent in the following that this inconsistency has strong implications for the dynamical evolution of the hot and dense matter produced in relativistic nuclear collisions.

It is instructive to consider the temperature dependence of the *pseudo-critical* pressure,  $p_{pc}$ , the pressure at which the phase transformation occurs. At subcritical temperatures,  $T < T_{crit}$ ,  $p_{pc}$  is obviously equal to the coexistence pressure, but in the cross-over region (*i.e.* above the critical temperature) the definition of  $p_{pc}$  is not unique (though different definitions yield qualitatively similar results). Essential differences between models are then brought out by the behavior of the transition pressure with temperature,  $p_{pc}(T)$ .

Figure 4 shows the temperature dependent pseudo-critical pressure for the two models considered here. For a specified temperature  $T$ ,  $p_{pc}^{HQ}$  is obtained by increasing

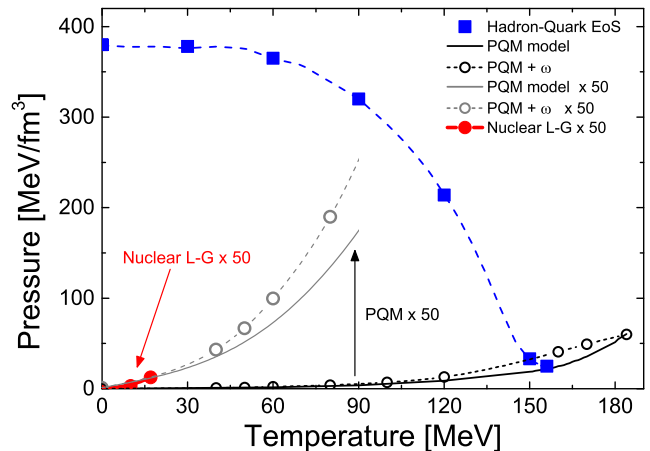


FIG. 4: (Color online) The pseudo-critical pressure as a function of the temperature,  $p_{pc}(T)$ , for both the HQ (blue dashed curve with squares) and the PQM model (black curves) models. The black dashed line with open circles shows the result of the PQM model with finite quark vector coupling. On a scale magnified by a factor of fifty, the PQM results (grey) are compared with the nuclear liquid-gas transition (which displays the familiar liquid-gas phase transition).

the chemical potential  $\mu$  until the ideal hadron-gas and the quark-gluon bag have the same pressure, while  $p_{pc}^{PQM}$  is taken as the pressure along the inflection point of the chiral condensate.

While the resulting pseudo-critical pressures are comparable at the highest temperatures (corresponding to  $\mu \approx 0$ ), and consistent with lattice results [46], they deviate strongly at large chemical potentials: As the temperature is reduced,  $p_{pc}^{HQ}$  increases steadily, as was already noted in previous studies employing models that describe the hadron-quark transition [23, 38]. By contrast,  $p_{pc}^{PQM}$  decreases steadily and vanishes at  $T = 0$ , a behavior that is a robust feature of the PQM models and persists also in the presence of a repulsive quark interaction [47, 48].

For comparison, Fig. 4 also shows the coexistence pressure for the liquid-gas phase transition in ordinary nuclear matter. It is quantitatively very similar to the low-temperature part of the corresponding PQM result. In particular, these pressures start from *zero* at  $T = 0$  and then *increase* steadily with  $T$ . This generic liquid-gas behavior differs qualitatively from the HQ result, for which the pressure *decreases* steadily with temperature.

This analysis suggests that the nature of the PQM phase transition resembles that of the nuclear liquid-gas transition and differs qualitatively from the quark-hadron transition. For the liquid-gas phase transition, the dense phase (the liquid) has fewer active degrees of freedom than the dilute phase (the vapor), so the liquid-to-gas transition increases the entropy per baryon. By contrast, for the confinement transition the entropy per baryon decreases because the dense system (the quark-gluon plasma) has more active degrees of freedom than

the coexisting dilute system (the hadron gas). Indeed, from the Clausius-Clapeyron relation it follows that a decrease in the entropy per baryon from the dense to the dilute phase requires that the pressure decrease with temperature [23], as exhibited in HQ EoS. It is important to keep this qualitative difference in mind.

While at present it is not known which class the QCD phase-transition belongs to, we note that recent lattice QCD calculations [6] have extracted the pressure at the crossover temperature  $T_\times = 153$  MeV and vanishing chemical potential to be  $p(T_\times, \mu = 0) \simeq 50$  MeV/fm<sup>3</sup>. This corresponds to the pressure of cold nuclear matter at a density of roughly three times the ground state density,  $\rho = 3\rho_s$  [49, 50]. Therefore, unless the hadron-quark transition happens at densities of  $\rho \simeq 3\rho_s$  or below, the pressure is expected to rise as we lower the temperature and increase the density, just as  $p_{\text{pc}}^{\text{HQ}}(T)$  in Fig. 4.

A further inspection of Fig. 4 shows that even though the HQ and PQM pseudo-critical pressures are numerically rather similar in the high-temperature region where  $\mu \approx 0$ , the slopes of  $p_{\text{pc}}^{\text{HQ}}(T)$  and  $p_{\text{pc}}^{\text{PQM}}(T)$  are opposite. Because this is the phase region that can be accessed by lattice QCD methods it would be interesting to investigate whether those can help to distinguish between the models. We therefore briefly discuss the prospects for this.

The introduction of the pseudo-critical pressure  $p_{\text{pc}}(T)$  makes it possible to define the associated pseudo-critical chemical potential  $\mu_{\text{pc}}(T)$  determined by  $p_{\text{pc}}(T) = p(T, \mu_{\text{pc}}(T))$ . In lattice QCD the inverse relationship,  $T_{\text{pc}}(\mu)$ , has been obtained to second order in  $\mu$  for various definitions of the pseudo-critical line [5, 6, 37],

$$T_{\text{pc}}(\mu) = T_\times \left[ 1 - \kappa \frac{\mu^2}{T_\times^2} \right], \quad (14)$$

where we recall that  $T_\times = T_{\text{pc}}(0)$  is the crossover temperature at  $\mu = 0$ . The curvature of the pseudo-critical line  $T_{\text{pc}}(\mu)$  depends on the definition of pseudo criticality. For example, if the inflection point of the chiral condensate is used then  $T_\times = 153$  MeV and  $\kappa = 0.0066$  [37]. On the other hand, if the inflection point of  $s/T^3$  is used (where  $s$  is the entropy density) then  $\kappa = 0.016$ , more than a factor of two larger, and  $T_\times = 158$  MeV, using the lattice EoS parametrization from Ref. [6].

In order to determine the slope of the pseudo-critical pressure, we use that  $p(T, \mu > 0)$  can be obtained by a Taylor expansion around  $\mu = 0$  [4, 8],

$$p(T, \mu) = p(T, \mu = 0) + T^4 \sum_{n>0} \frac{\chi_{2n}(T)}{(2n)!} \left( \frac{\mu}{T} \right)^{2n}. \quad (15)$$

The Taylor coefficients  $\chi_n(T)$  are the  $n$ 'th-order baryon-number susceptibilities evaluated at vanishing  $\mu$ ,

$$\chi_n(T) = \frac{\partial^n}{\partial (\mu/T)^n} \frac{p}{T^4} \Big|_{\mu=0}. \quad (16)$$

Thus, for sufficiently small values of  $\mu_{\text{pc}}$ , the pseudo-critical pressure,  $p_{\text{pc}}(T) = p(T, \mu_{\text{pc}}(T))$ , is given by

$$p_{\text{pc}}(T) = p(T, \mu = 0) + T^4 \sum_{n>0} \frac{\chi_{2n}(T)}{(2n)!} \left( \frac{\mu_{\text{pc}}(T)}{T} \right)^{2n}. \quad (17)$$

To second order in  $\mu_{\text{pc}}$  this can be evaluated using Eq. (14). In particular, the slope of the pseudo-critical pressure at  $\mu = 0$  is given by

$$\frac{\partial}{\partial T} p_{\text{pc}}(T, \mu = 0) \Big|_{T=T_\times} = s(T_\times, \mu = 0) - \frac{T_\times^3}{2\kappa} \chi_2(T_\times). \quad (18)$$

The entropy density,  $s$ , the curvature of the pseudo-critical line,  $\kappa$ , and the second-order susceptibility,  $\chi_2$ , have been calculated on in lattice QCD with physical quark masses and in the continuum limit [6, 51]. Using those values, we then find that the sign of the above slope depends on the definition of the pseudo criticality. If it is defined by the inflection points of either the chiral condensate or the strangeness susceptibility we find the slope of the pressure along the pseudo-critical to be  $\partial_T p_{\text{pc}} = -2.3T_\times^3$  or  $\partial_T p_{\text{pc}} = -1.1T_\times^3$ , respectively. In both case the slope is negative meaning the pressure increases as we decrease the temperature, similar to the HQ result depicted in Fig. 4. If, on the other hand, the pseudo-critical line is defined by the inflection point of  $s/T^3$ , the slope of the pseudo-critical pressure turns out to be positive,  $\partial_T p_{\text{pc}} = +2.4T_\times^3$ . This is a simple consequence of the fact that the curvature of the pseudo-critical line,  $\kappa$ , is a more than a factor of two larger in this case.

Thus, from the above considerations we must, regrettably, conclude that at present lattice QCD calculations cannot distinguish between the two scenarios at hand: a liquid-gas type behavior where the pseudo-critical pressure increases with temperature or a decreasing behavior as is suggested by phenomenology and implemented in the HQ EoS used in the present study.

#### IV. FLUID DYNAMICAL CLUMPING

Next we employ the two equations of state in dynamical calculations and look for qualitative and quantitative differences between the results. Specifically, we employ ideal fluid dynamics to study systems as they expand through the unstable phase region. Dissipative effects are not expected to play a decisive role for the spinodal clumping [38], because even though the inclusion of viscosity generally tends to slow the growth, the dissipative mechanisms also lead to heat conduction which has the opposite effect and also enlarges the unstable region. The equations of motion derived from conservation of four-momentum and net baryon number are solved by means of the code SHASTA [52] in which the propagations in the three spatial dimensions are carried out consecutively.

In order to obtain a proper description of the spinodal growth rates in the mechanically unstable region of the

phase diagram, it is essential to introduce finite-density effects [29, 38]. This was done in Ref. [35] by augmenting the pressure obtained from the EoS,  $p_0(\varepsilon, \rho)$ , by a gradient term,  $\delta p(\mathbf{r}) = -a^2 \rho(\mathbf{r}) \nabla^2 \rho(\mathbf{r}) \varepsilon_s / \rho_s^2$ , so the local pressure is given by  $p(\mathbf{r}) = p_0(\varepsilon(\mathbf{r}), \rho(\mathbf{r})) + \delta p(\mathbf{r})$ . For the HQ EoS, the resulting simulation tool was verified to yield the correct growth rates of the mechanical instabilities in the spinodal phase region [35]. Furthermore, it was found that the associated spinodal instabilities may cause significant amplification of initial density irregularities in relativistic lead-lead collisions [35, 36].

We use this tool to investigate the effect of the different equations of state on observables for the QCD phase transition at large baryon densities. To facilitate the comparisons, we employ the same range  $a$  in the gradient term also for the PQM EoS (namely  $a = 0.033$  fm) which then yields a significantly smaller surface tension (namely  $\approx 2$  MeV/fm<sup>2</sup> and compared to  $\approx 10$  MeV/fm<sup>2</sup> for the HQ EoS). This is not surprising because the PQM densities tend to be smaller, as then also the differences between the coexistence densities are, and the PQM EoS looks rather similar to the LG EoS which has a smaller surface tension (namely  $\approx 1$  MeV/fm<sup>2</sup>).

In particular, we will study the evolution of spherically symmetric systems, where the energy and baryon densities ( $\varepsilon$  and  $\rho$ ) are initialized according to a Woods-Saxon distribution,

$$\varepsilon(\mathbf{r}) = \varepsilon_I [1 + e^{(r-c)/w}]^{-1}, \quad (19)$$

$$\rho(\mathbf{r}) = \rho_I [1 + e^{(r-c)/w}]^{-1}, \quad (20)$$

where  $r$  is the distance to the center and  $\varepsilon_I$  and  $\rho_I$  are the corresponding central density values. For the radius we use  $c = 4$  fm and the width parameter is  $w = 0.5$  fm. To provide initial seeds of fluctuations to be amplified, we modify the density profile by adding random fluctuations  $\delta\varepsilon(\mathbf{r})$  and  $\delta\rho(\mathbf{r})$  to the local densities,  $\varepsilon(\mathbf{r})$  and  $\rho(\mathbf{r})$ . The amplitudes of the fluctuations are constrained to a maximum of  $\pm 20\%$  of the corresponding local densities (19) and they are uniformly distributed within this range.

For both equations of state, we initialize the system at a temperature of 100 MeV and a density that corresponds to a phase point  $(\varepsilon, \rho)$  slightly above the unstable region (for the PQM EoS) or just inside the unstable region (for the HQ EoS). We obtain the strongest ‘clumping’ when the system is initialized inside the spinodal region. For the PQM model such a system would have negative pressure, as shown in Fig. 3. Consequently, the system will grow denser until its phase point leaves the unstable region and the pressure turns positive. Because this initial compression delays the eventual dynamical expansion, the PQM calculation is initialized already at a density above the unstable region, thus eliminating the delay that would otherwise be caused by the negative pressure.

As the system evolves, we extract several quantities that might be sensitive to the developing instabilities. To establish a suitable reference, we also let the systems

evolve from the same initial state but with the corresponding stable EoS obtained by eliminating the phase-transition instabilities by means of Maxwell constructions, thus preserving the features outside the phase-coexistence region.

For the PQM EoS, Fig. 5(a) shows the initial density distribution in the  $xy$  plane, as obtained by augmenting Eqs. (19-20) by fluctuations. This initial state is then evolved with ideal fluid dynamics (with the gradient term included) using the unstable EoS. The resulting density distribution after 160 fm/c is shown in Fig. 5(b). Even after such a long time one finds meta-stable clusters of high baryon density with an asymmetric angular distribution, an observation that was first reported in [44]. This phenomenon is a direct consequence of the liquid-gas nature of the PQM model, which predicts phase coexistence between the dense phase and the vacuum at vanishing temperature. As a consequence, the pressure even at  $T = 100$  MeV is very small (see Fig. 2) resulting in a slow expansion. In addition, due to the small pressure difference between the dense phase and the vacuum, the clusters generated during the unstable stage are nearly stable and therefore live for a long time, before they eventually slowly disappear on a timescale of hundreds of fm/c.

The situation is quite different in case of the HQ EoS. As in the calculation based on the PQM EoS, the fluctuations are quickly amplified to form small clusters, illustrated in Fig. 6(a). However, in contrast to the PQM, the QGP clusters disappear rather quickly after the surrounding hadronic matter expands and dilutes. This is due to the very high pressure difference between the dense phase and the vacuum, as depicted in Fig. 1. The diluted density distribution, after a time of only 10 fm/c, is shown in Fig. 6(b), where it is evident that the previously formed dense clusters have been completely washed out.

Consequently, the two scenarios, PQM and HQ, exhibit the same qualitative features but lead to quantitatively different time scales and amplitudes. It is therefore useful to now estimate the quantitative differences in observables resulting from the two equations of state.

## V. OBSERVABLES

In this section we investigate the sensitivity of various proposed observables to the formation of clusters of deconfined matter.

### A. Powers of the density

The density moments provide a convenient global quantification the irregularities in the evolving net baryon density  $\rho(\mathbf{r}, t)$  [35],

$$\langle \rho(t)^N \rangle \equiv \frac{1}{A} \int \rho(\mathbf{r}, t)^N \rho(\mathbf{r}, t) d^3\mathbf{r}, \quad (21)$$

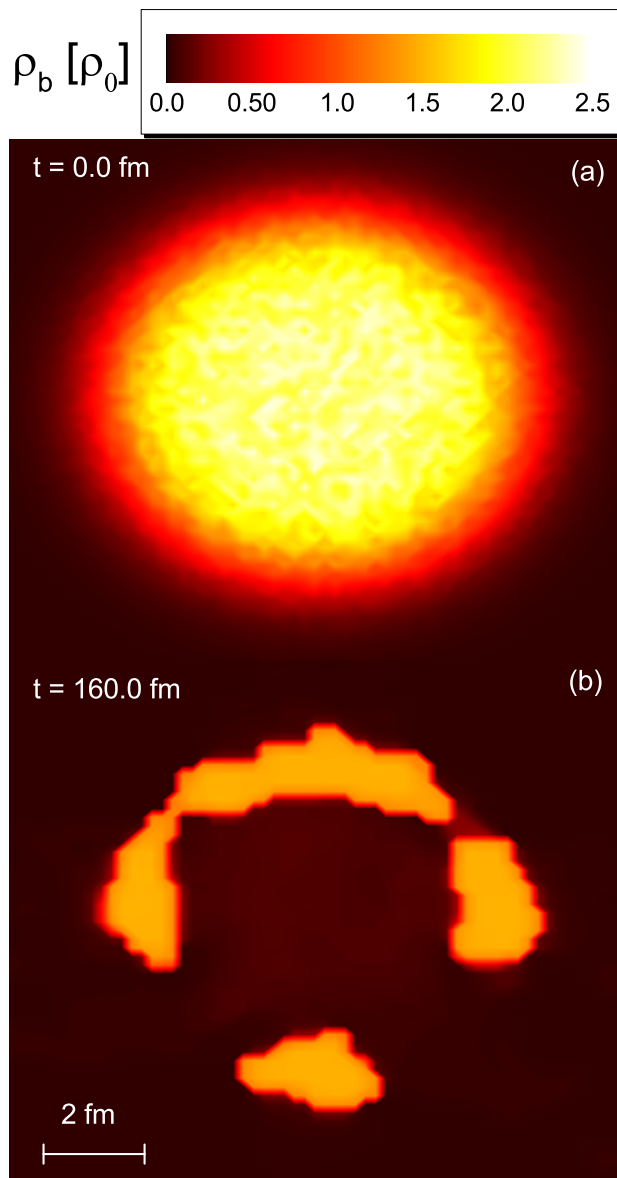


FIG. 5: (Color online) (a): Initial net baryon density distribution in the  $x$ - $y$  plane. The initial state is constructed to lie just above the unstable region of the PQM equation of state. (b): Net baryon density distribution in the  $x$ - $y$  plane after  $160 \text{ fm}/c$  evolution with the PQM equation of state, that has an unstable region. The clusters of high baryon density are clearly visible.

where  $A = \int \rho(\mathbf{r}, t) d^3\mathbf{r}$  is the (constant) net baryon number of the system. As already shown in Ref. [35], the higher moments are more sensitive to the magnitude of the fluctuations and we show results for  $N = 5$  here.

Figure 7 shows the time evolution of the fifth density moment, divided by its initial value  $\langle \rho(t=0)^5 \rangle$ , for the two different equations of state considered.

For the HQ EoS the instabilities in the coexistence region lead to local density enhancements which manifest themselves in the bump of the density moment. Rela-

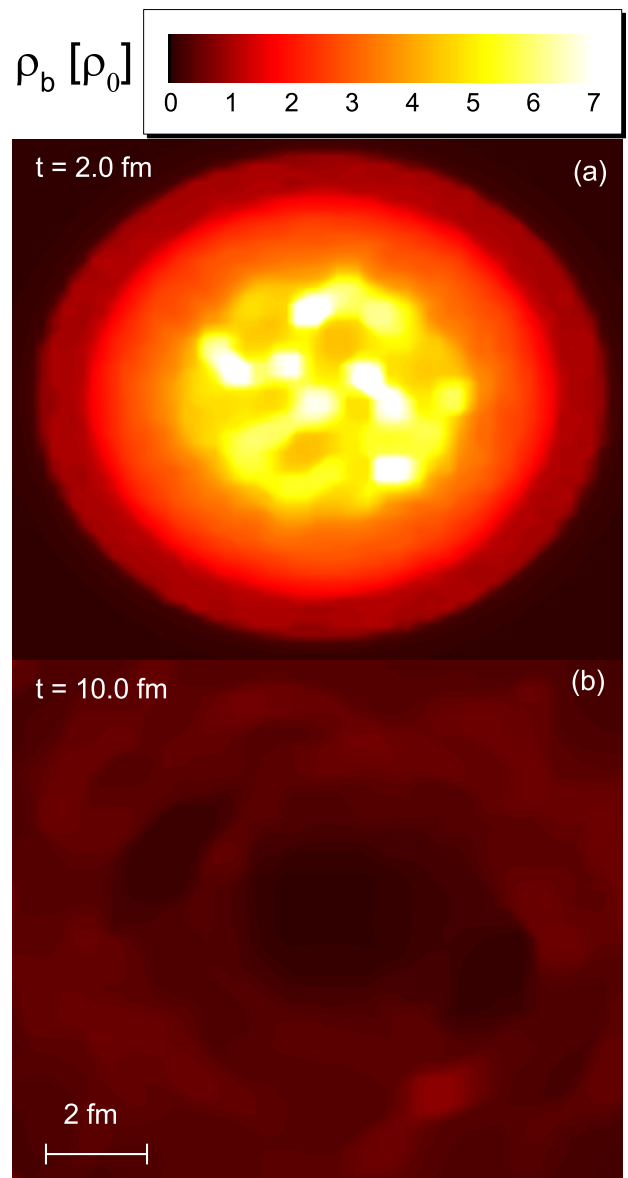


FIG. 6: (Color online) The net baryon density in the  $xy$  plane,  $\rho(x, y, 0, t)$ , after  $t = 2 \text{ fm}/c$  (a) and  $t = 10 \text{ fm}/c$  (b), as obtained with the unstable HQ EoS: Clumps of dense quark matter are formed at early times (a) but they disappear after further evolution (b).

tive to the evolution with the Maxwell partner EoS, the maximum enhancement of the fifth density moment is about a factor of 3-4. But once the surrounding medium has become sufficiently dilute these clumps again dissolve resulting in a rapid drop of the density moment. The largest degree of enhancement occurs when most of the system is inside the unstable phase region. After the system leaves this region the density quickly becomes similar to that obtained with the stable partner EoS.

The PQM EoS yields a quite different picture. Because of the low pressure at the phase-coexistence line, the dynamical evolution is considerably slower and the



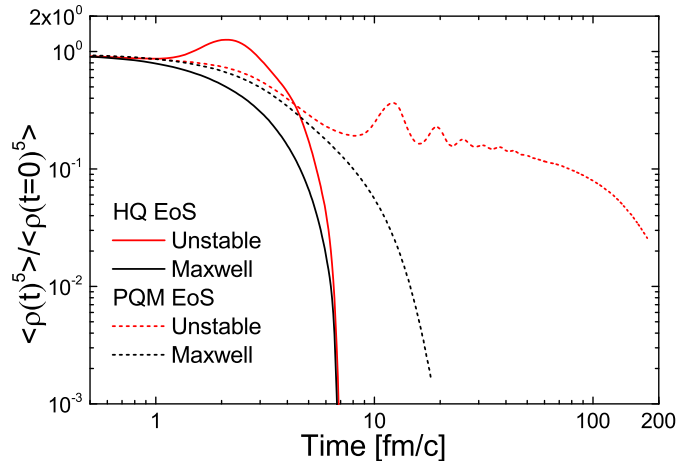


FIG. 7: (Color online) The fifth density moment (see Eq. (21)), normalized to its initial value, as a function of time for the HQ (solid) and the PQM (dashed) EoS. In each case, the upper curve (red) depicts results obtained with the unstable EoS, while the lower curve (black) has been obtained with the corresponding Maxwell partner EoS.

density moment starts to increase only after a long time. And because the created clumps are almost stable, and only decay very slowly when embedded in a very dilute gas, the density enhancements become much larger than was the case for the HQ EoS. This qualitative difference is clearly brought out in Fig. 7 for the fifth density moment. We also note its oscillatory behavior which can be ascribed to the longevity of the created clusters: As the clusters are formed, the inflowing baryon current will over-compress the dense quark droplet which in turn will cause it to subsequently expand slowly bringing it again slightly inside the unstable region, thus causing a second (somewhat weaker) over-compression and so on.

The calculation also shows that the PQM density moment starts to decrease appreciably only after a very long time (100 – 200 fm). A similar slow decrease of the PQM density moments was also observed in a different simulation [44]. This clearly shows how the liquid-gas type properties of the deconfinement transition implied by the PQM EoS may yield potentially misleading results.

## B. Composite production

Another potential signal observable is the production yield of composite particles (*i.e.* light nuclei such as deuterons and tritons) from phase-space coalescence of nucleons. In the simple coalescence picture, the phase-space density of a composite with baryon number  $A$  is proportional to the  $A$ 'th power of the one-particle nucleon phase-space density [53–57]. Therefore, because the spinodal instabilities significantly enhance higher powers of the density, as demonstrated in Fig. 7, one might naively expect that the composite production should be

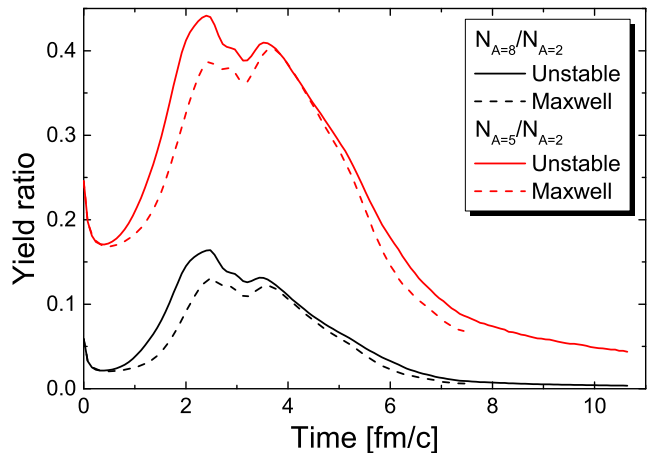


FIG. 8: (Color online) The ratios of the  $A = 5$  and  $A = 8$  nuclei over the deuteron yield as functions of time. For simplicity, the degeneracy factors for  $A = 8$ ,  $A = 5$ , and  $A = 2$  have been set to equal values. Shown are results for the HQ equation of state with an unstable region (solid lines) and with a Maxwell construction (dashed lines).

enhanced. However, as the local baryon density is being enhanced also the local excitation energy per baryon is increased and that will decrease in the coalescence yield, almost compensating the increase due to the higher density, as we shall demonstrate below.

First let us recall that the coalescence model gives the production yield in terms of the nucleon yield as [53–57],

$$E_A \frac{dN_A}{d^3\mathbf{P}_A} \propto F_A \left( \left[ E \frac{dn}{d^3\mathbf{p}} \right]_{\mathbf{p}=\mathbf{P}_A/A} \right)^A. \quad (22)$$

Here  $F_A$  is a coalescence factor related to the quantum mechanical overlap integral between the wave functions of the parent nucleons and the composite to be formed; it depends only weakly on  $A$ . Given the simple assumptions made in this work, *e.g.* for the initial conditions, a calculation of the absolute yield of composite nuclei is not warranted. Instead we focus on the relative composite yields in the presence or absence of spinodal instabilities.

This simplifies our calculation considerably, because Ref. [53] showed that for a non-degenerate system the coalescence yield and the thermal production yield are identical up to factors involving the coalescence radius and the binding energy of the composites. Because these factors will be the same in all scenarios we are considering, we should get a good estimate for the relative enhancement by simply integrating the local thermal composite populations. To this end, we apply the Cooper-Frye prescription on an isochronous hypersurface, using values of the temperature and chemical potential of a hadron gas corresponding to the local energy and baryon densities. The total population of light nuclei with mass number  $A$

is then given by

$$N_A = \int d^3\mathbf{p} d^3\mathbf{r} f_A(\mathbf{r}, \mathbf{p}), \quad (23)$$

with  $f_A(\mathbf{r}, \mathbf{p}) \propto \exp[-(\sqrt{m_A^2 + p^2} - \mu_A(\mathbf{r}))/T(\mathbf{r})]$ , where we have used an effective degeneracy of one because we are interested only in ratios. Furthermore, we assume that  $\mu_A(\mathbf{r}) = A\mu(\mathbf{r})$  and  $m_A = Am_N$ , where  $m_N$  is the nucleon mass. Figure 8 shows the number of composites with baryon number  $A = 5$  and  $A = 8$  relative to the deuteron yield ( $A = 2$ ). It is obvious that the relative composite populations increase at the time when the baryon density is enhanced, *i.e.* when the moments of the baryon number distributions increase. However, the increase in the population of composite nuclei is much smaller than the increase in the density moments. Indeed, we observe a maximum increase in the relative composite production of only up to 20%, as compared to what is obtained with the corresponding Maxwell EoS.

### C. Angular correlations

As can be seen from Fig. 5, there seems to be strong irregularities in the angular distribution of the baryon density in the case of strong clumping. It has been asserted in [44] that this will lead to large higher moments of the spacial angular distribution of the baryon number. In this section we will investigate the angular irregularities further by calculating the two-particle angular correlations of baryons, in both coordinate and momentum space.

In position space these can be computed directly from the fluid dynamical simulations,

$$V_n^{\text{pos}} = \frac{1}{N^2} \sum_{i,j=1}^N \rho_i \rho_j \cos(n(\phi_i^{\text{pos}} - \phi_j^{\text{pos}})), \quad (24)$$

where  $\rho_i$  is the net baryon density at the computational lattice point  $i$ ,  $\phi_i^{\text{pos}}$  is its azimuthal angle, and  $N = \sum_i \rho_i$ .

However, experiments usually measure the momentum-space asymmetries  $v_n$  and momentum correlations rather than coordinate-space asymmetries. The azimuthal momentum distribution of the emitted particles is commonly expressed as

$$\frac{dN}{d\Phi^{\text{mom}}} \propto 1 + \sum_{n=1}^{\infty} 2v_n \cos(n(\Phi^{\text{mom}} - \Psi_n)) \quad (25)$$

where  $v_n$  is the magnitude of the  $n$ 'th order harmonic term relative to the angle of the initial-state spatial plane of symmetry  $\Psi_n$ . To calculate the two-baryon correlations in momentum space we need the relative angle between the momenta of baryons coming from the cells  $i$  and  $j$ ,  $\Phi_{ij}^{\text{mom}}$ ,

$$V_n^{\text{mom}} = \frac{1}{N_{ij}} \sum_{ij} \rho_i \rho_j \cos(n\Delta\Phi_{ij}^{\text{mom}}). \quad (26)$$

The angle of the momentum of a baryon coming from cell  $i$  is determined by sampling the Cooper-Frye equation [58, 59] with the local values of four velocity  $u_\nu$ , temperature  $T$ , and chemical potential  $\mu$ . This method will create a statistical uncertainty which can be minimized by making multiple samplings of  $V_n^{\text{mom}}$  and averaging Eq. (26) over all samplings.

It can be shown [60, 61] that the extracted correlation measures  $V_n^{\text{mom}}$  are related to the squares of the Fourier coefficients of the angular distributions:

$$V_n^{\text{mom}} = v_n^2 \quad (27)$$

assuming no corrections due to momentum conservation and resonance decays. Figures 9 and 10 show our results for the coordinate and momentum space angular correlations. We compare results with the PQM model, at the end of the evolution (see figure 7), and the HQ model, also at the end of the evolution.

As expected from Ref. [44], the coordinate-space correlations from the PQM model are very large when the system goes through the unstable region. As shown in section IV, using the unstable PQM equation of state will create large quark clusters, containing most of the system's baryon number. This of course leads to strong correlations in coordinate-space and several moments are even larger than 10%. When the Maxwell constructed equation of state is used no clusters are formed and the baryon matter is distributed more homogeneously in coordinate-space, resulting in no strong spacial correlations.

The calculation with the HQ model shows much smaller coordinate-space correlations, of at most 2–3%. This result is also understandable, as the produced clusters contain only a small fraction of the system's baryon number and quickly become unstable and expand. However, the clumping obtained with the unstable EoS is still larger than with the corresponding Maxwell construction which again showed no density enhancement.

Figure 10 shows how these coordinate-space irregularities are transformed into momentum-space correlations. The high pressure along the coexistence line in the HQ model leads to an efficient translation of coordinate space irregularities into momentum space. Importantly, the difference between the unstable EoS and the Maxwell EoS is not very large. Only a factor 1.4 increase in the momentum correlation amplitude is observed. The considerable increase in the baryon density, due to the clumping in our simulations with the unstable EoS, does not lead to a considerable change in the pressure gradients. Consequently, the additional spacial anisotropies are not reflected strongly in the final momentum anisotropies.

Due to the small pressure in the PQM equation of state, the coordinate-space asymmetries here cause even less momentum-space asymmetries, which is already seen for the Maxwell constructed EoS that has no instabilities. Even after an evolution time of 160 fm, which is much longer than the expected lifetime of the fireball, the un-

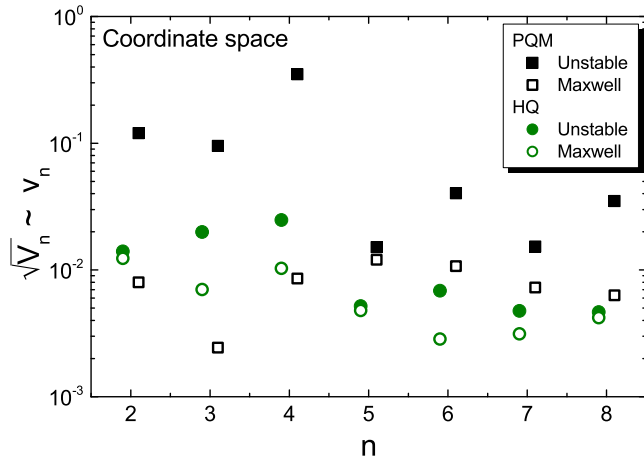


FIG. 9: (Color online) The position-space two-baryon angular correlation strength  $V_n^{\text{pos}}$  for various values of  $n$  as obtained with the HQ (circles) and PQM (squares) EoS. The results obtained with an unstable EoS (solid) are contrasted with those employing the Maxwell partner (open).

stable PQM EoS shows no strong angular momentum-space correlations, even though it had very large angular correlations in coordinate space.

## VI. SUMMARY

We have investigated the effect of qualitatively different types of two-phase equation of state on the expansion dynamics and on possible experimental signals of the expected QCD phase transition at large baryon densities. We considered two equations of state representing two qualitatively different EoS classes. On the one hand, as an example for an EoS exhibiting phase coexistence between compressed nuclear matter and the dense quark phase, we considered an EoS that is constructed by interpolating between a hadron gas and a quark-gluon phase. On the other hand, as a representative for the class of liquid-gas type equations of state, we used the EoS from a PQM-like model.

We find that the PQM model shows a transition that is very similar to that of the liquid-gas transition in nuclear matter and thus this model differs qualitatively from the HQ model with regard to the thermodynamic properties near the phase coexistence line. We also compared the effective equations of state with a Taylor expansion of recent lattice QCD data. Unfortunately, the predicted slope of the pressure along the pseudo-critical line at vanishing chemical potential depends of the specific definition of pseudo criticality. Therefore, at present lattice results are not able to discriminate between the liquid-gas type behavior of the PQM equation of state and the HQ equation of state. This is unfortunate, as the two types of EoS yield dramatically different pressures in the high- $\mu$  region.

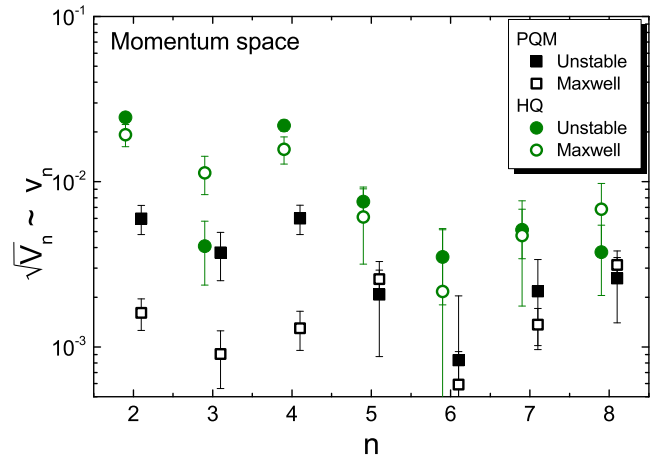


FIG. 10: (Color online) The momentum-space two-baryon angular correlation strength  $V_n^{\text{mom}}$  for various values of  $n$  as obtained with the HQ (circles) and PQM (squares) EoS. The results obtained with an unstable EoS (solid) are contrasted with those employing the Maxwell partner (open).

The qualitative differences between the two equations of state examined in this work lead to significant quantitative differences in the time evolution of fireballs that expand through the respective unstable region of the phase diagram. In the PQM model the lifetime of quark clusters is orders of magnitude longer than what is usually expected for the timescales of heavy-ion collisions and it predicts stable dense quark matter droplets at zero temperature, i.e. coexisting with the vacuum.

The instabilities associated with the presence of a first-order phase transition lead to large irregularities in the spatial distribution of the baryon number. However, these irregularities are not translated into significant momentum correlations. We also show that quark cluster formation only leads to an small increase in the production of composite nuclei, of less than 20%. This increase is only observed when the system is inside the unstable region. Once the system has left the coexistence region and dispersed all signals seem washed out.

In conclusion, we have shown that the qualitative differences between the PQM and HQ equations of state lead to considerable differences in the dynamical evolution of the system. Given the arguments provided in this paper, we believe that these qualitative differences persist independent of the specific EoS model adopted of either the LG type or a more plausible type. However, the observation of these differences is a challenging task. The two rather intuitive observables explored here have shown little sensitivity to either the instabilities associated with the first-order phase co-existence or the dynamical evolution of the system. Thus the key question on how to detect those instabilities, if indeed present, remains unsettled.

Furthermore, the qualitative behavior of the pressure along the pseudo-critical line in the QCD phase plane

is not yet known. Lattice QCD calculations of higher-order Taylor coefficients for the pseudo-critical line and the associated pressure might help to clarify this crucial issue. Meanwhile, as long as it remains an open question whether the pseudo-critical pressure increases or decreases, both possibilities must be considered when validating any potential phase-transition signal with dynamical calculations similar to the ones presented here.

## VII. ACKNOWLEDGMENTS

The authors would like to thank M. Prakash for discussions regarding the equation of state of neutron stars. VK

would like to thank the EMMI Rapid Reaction Task Force on “Probing the Phase Structure of Strongly Interacting Matter with Fluctuations” where some of the ideas for this work were initiated. This work was supported by GSI and Hessian initiative for excellence (LOEWE) through the Helmholtz International Center for FAIR (HIC for FAIR) and by the Office of Nuclear Physics in the U.S. Department of Energy’s Office of Science under Contract No. DE-AC02-05CH11231. JS was supported in part by the Alexander von Humboldt Foundation as a Feodor Lynen Fellow.

- 
- [1] Y. Aoki, G. Endrodi, Z. Fodor, S. D. Katz, and K. K. Szabo, *Nature* **443**, 675 (2006).
- [2] Y. Aoki, Z. Fodor, S. D. Katz, and K. K. Szabo, *Phys. Lett. B* **643**, 46 (2006).
- [3] A. Bazavov *et al.*, *Phys. Rev. D* **85**, 054503 (2012).
- [4] C. R. Allton *et al.*, *Phys. Rev. D* **66**, 074507 (2002).
- [5] O. Kaczmarek *et al.*, *Phys. Rev. D* **83**, 014504 (2011).
- [6] S. Borsanyi, G. Endrodi, Z. Fodor, S. D. Katz, S. Krieg, C. Ratti, and K. K. Szabo, *JHEP* **1208**, 053 (2012).
- [7] S. Borsanyi, Z. Fodor, S. D. Katz, S. Krieg, C. Ratti, and K. K. Szabo, *Phys. Rev. Lett.* **111**, 062005 (2013).
- [8] R. V. Gavai and S. Gupta, *Phys. Rev. D* **78**, 114503 (2008).
- [9] P. de Forcrand and O. Philipsen, *JHEP* **0811**, 012 (2008).
- [10] Z. Fodor and S. D. Katz, *JHEP* **0203**, 014 (2002).
- [11] Z. Fodor and S. D. Katz, *JHEP* **0404**, 050 (2004).
- [12] K. Fukushima, *Phys. Lett. B* **591**, 277 (2004).
- [13] C. Ratti, M. A. Thaler, and W. Weise, *Phys. Rev. D* **73**, 014019 (2006).
- [14] B. J. Schaefer, J. M. Pawłowski, and J. Wambach, *Phys. Rev. D* **76**, 074023 (2007).
- [15] J. M. Pawłowski, *Annals Phys.* **322**, 2831 (2007).
- [16] J. Berges, N. Tetradis, and C. Wetterich, *Phys. Rept.* **363**, 223 (2002).
- [17] B. J. Schaefer and J. Wambach, *Phys. Part. Nucl.* **39**, 1025 (2008).
- [18] T. K. Herbst, J. M. Pawłowski, and B. -J. Schaefer, *Phys. Rev. D* **88**, 0145007 (2013).
- [19] J. Steinheimer, S. Schramm, and H. Stöcker, *J. Phys.* **G38**, 035001 (2011).
- [20] L. Turko, D. Blaschke, D. Prorok, and J. Berdermann, *J. Phys. Conf. Ser.* **455**, 012056 (2013).
- [21] J. Steinheimer, S. Schramm, and H. Stöcker, *Phys. Rev. C* **84**, 045208 (2011).
- [22] V. Dexheimer, J. Steinheimer, R. Negreiros, and S. Schramm, *Phys. Rev. C* **87**, 015804 (2013).
- [23] M. Hempel, V. Dexheimer, S. Schramm, and I. Iosilevskiy, *Phys. Rev. C* **88**, 014906 (2013).
- [24] L. Ferroni, V. Koch and M. B. Pinto, *Phys. Rev. C* **82**, 055205 (2010) [arXiv:1007.4721 [nucl-th]].
- [25] I. C. Arsene, L. V. Bravina, W. Cassing, Y. .B. Ivanov, A. Larionov, J. Randrup, V. N. Russkikh, and V. D. Toneev, *Phys. Rev. C* **75**, 034902 (2007).
- [26] Ph. Chomaz, M. Colonna, and J. Randrup, *Phys. Rep.* **389**, 263 (2004).
- [27] J. Randrup, *Phys. Rev. Lett.* **92**, 122301 (2004).
- [28] C. Sasaki, B. Friman, and K. Redlich, *Phys. Rev. Lett.* **99**, 232301 (2007).
- [29] J. Randrup, *Phys. Rev. C* **79**, 054911 (2009).
- [30] J. Randrup, *Acta Phys. Hung. A* **22**, 69 (2005).
- [31] I. N. Mishustin, *Phys. Rev. Lett.* **82**, 4779 (1999).
- [32] D. Bower and S. Gavin, *Phys. Rev. C* **64**, 051902 (2001).
- [33] K. Paech, H. Stöcker, and A. Dumitru, *Phys. Rev. C* **68**, 044907 (2003).
- [34] M. Nahrgang, S. Leupold, C. Herold, and M. Bleicher, *Phys. Rev. C* **84**, 024912 (2011).
- [35] J. Steinheimer and J. Randrup, *Phys. Rev. Lett.* **109**, 212301 (2012).
- [36] J. Steinheimer and J. Randrup, *Phys. Rev. C* **87**, 054903 (2013).
- [37] G. Endrodi, Z. Fodor, S. D. Katz, and K. K. Szabo, *JHEP* **1104**, 001 (2011).
- [38] J. Randrup, *Phys. Rev. C* **82**, 034902 (2010).
- [39] E. Megias, E. Ruiz Arriola, and L. L. Salcedo, *Phys. Rev. D* **74**, 065005 (2006).
- [40] S. Roessner, C. Ratti, and W. Weise, *Phys. Rev. D* **75**, 034007 (2007).
- [41] C. Sasaki, B. Friman, and K. Redlich, *Phys. Rev. D* **75**, 074013 (2007).
- [42] S. K. Ghosh, T. K. Mukherjee, M. G. Mustafa, and R. Ray, *Phys. Rev. D* **73**, 114007 (2006).
- [43] K. Fukushima, *Phys. Rev. D* **77**, 114028 (2008) [Erratum-ibid. *D* **78**, 039902 (2008)].
- [44] C. Herold, M. Nahrgang, I. Mishustin, and M. Bleicher, arXiv:1304.5372 [nucl-th].
- [45] C. Herold, M. Nahrgang, I. Mishustin, and M. Bleicher, *Phys. Rev. C* **87**, 014907 (2013).
- [46] S. Borsanyi *et al.*, *JHEP* **1011**, 077 (2010).
- [47] O. Lourenco, M. Dutra, A. Delfino and M. Malheiro, *Phys. Rev. D* **84**, 125034 (2011).
- [48] M. B. Pinto, V. Koch and J. Randrup, *Phys. Rev. C* **86**, 025203 (2012).
- [49] M. Prakash, Lecture Notes of the workshop on the *The Nuclear Equation of State*, Jan 4 – 14, 1994, Puri, India,

- A. Ansari and L. Satpathy (eds), (World Scientific, 1996) pp: 229-410.
- [50] M. Prakash, T. L. Ainsworth and J. M. Lattimer, Phys. Rev. Lett. **61**, 2518 (1988).
- [51] S. Borsanyi, Z. Fodor, S. D. Katz, S. Krieg, C. Ratti, and K. Szabo, JHEP **1201**, 138 (2012).
- [52] D. H. Rischke, S. Bernard, and J. A. Maruhn, Nucl. Phys. A **595**, 346 (1995).
- [53] L. P. Csernai and J. I. Kapusta, Phys. Rept. **131**, 223 (1986).
- [54] C. B. Dover, P. Koch, and M. May, Phys. Rev. C **40**, 115 (1989).
- [55] H. Sato and K. Yazaki, Phys. Lett. B **98**, 153 (1981).
- [56] C. B. Dover, U. W. Heinz, E. Schnedermann, and J. Zimanyi, Phys. Rev. C **44**, 1636 (1991).
- [57] R. Scheibl and U. W. Heinz, Phys. Rev. C **59**, 1585 (1999).
- [58] F. Cooper and G. Frye, Phys. Rev. D **10**, 186 (1974).
- [59] H. Petersen, J. Steinheimer, G. Burau, M. Bleicher, and H. Stöcker, Phys. Rev. C **78**, 044901 (2008).
- [60] M. Luzum, Phys. Lett. B **696**, 499 (2011).
- [61] K. Aamodt *et al.* [ALICE Collaboration], Phys. Lett. B **708**, 249 (2012).